Antiviral Research 100 (2013) 356–364

Contents lists available at ScienceDirect

Antiviral Research

journal homepage: www.elsevier.com/locate/antiviral

Insights into susceptibility of antiviral drugs against the E119G mutant of 2009 influenza A (H1N1) neuraminidase by molecular dynamics simulations and free energy calculations

Peichen Pan [a], Lin Li [a], Youyong Li [a], Dan Li [b,*], Tingjun Hou [a,b,*]

[a] Institute of Functional Nano & Soft Materials (FUNSOM) and Jiangsu Key Laboratory for Carbon-Based Functional Materials & Devices, Soochow University, Suzhou, Jiangsu 215123, China
[b] College of Pharmaceutical Sciences, Zhejiang University, Hangzhou, Zhejiang 310058, China

ARTICLE INFO

Article history:
Received 14 August 2013
Revised 7 September 2013
Accepted 10 September 2013
Available online 19 September 2013

Keywords:
Influenza viruses
H1N1
Neuraminidase inhibitors
Drug resistance
Molecular dynamics simulations
MM/GBSA

ABSTRACT

Neuraminidase inhibitors (NAIs) play vital roles in controlling human influenza epidemics and pandemics. However, the emergence of new human influenza virus mutant strains resistant to existing antiviral drugs has been becoming a major challenge. Therefore, it is critical to uncover the mechanisms of drug resistance and seek alternative treatments to combat drug resistance. In this study, molecular dynamics (MD) simulations and Molecular Mechanics/Generalized Born Surface Area (MM/GBSA) were applied to investigate the different sensitivities of oseltamivir (OTV), zanamivir (ZNV), and peramivir (PRV) against the E119G mutant of 2009 A/H1N1 neuraminidase. The predicted binding free energies indicate that the E119G mutation in NA confers resistance to all of the three studied inhibitors. The ordering of the level of drug resistance predicted by the binding free energies for the three inhibitors is ZNV > PRV > OTV, which agrees well with the experimental data. Drug resistance arises primarily from the unfavorable shifts of the polar interactions between NA and the inhibitors. It comes as a surprise that the mutation of Glu119 that can form strong H-bonds with the inhibitors in the wild-type protein does not have direct impact on the binding affinities of both OTV and PRV due to the regulation of the strong unfavorable polar desolvation energies. The indirectly conformational variations of the inhibitors, which caused by the E119G mutation, are responsible for the loss of the binding free energies. However, for ZNV, the E119G mutation has both direct and indirect influences on the drug binding. The structural and quantitative viewpoint obtained from this study provides valuable information for the rational design of novel and effective drugs to combat drug resistance.

1. Introduction

In the last century, since human influenza pandemic at the first time occurred in 1918 (Spanish, A/H1N1), influenza viruses have already killed millions of people (Hsieh et al., 2006; Palese, 2004). In recent years, two types of influenza virus, A/H5N1 (avian flu) (Ferguson et al., 2004; Yen and Webster, 2009) and A/H1N1 (swine flu) (Neumann et al., 2009; Organization, 2009), have outbroken and spread all over the world. At the moment, the new subtype 2009 Influenza A (H1N1), which is a recombined virus derived from human, swine, and avian influenza viruses, with high transmissible ability among human beings is continually mutating (Garten et al., 2009), while no one can predict when the next pandemic will occur.

There are two principal glycoproteins on the surface of the virus particles, hemagglutinin (HA) and neuraminidase (NA), which are both targets of the neutralizing antibodies immune response (Arias et al., 2009; Organization, 1980). As the virus approaches a cell, HA plays a starring role in binding to the sialic acid receptor on the cell surface and facilitating the entry of influenza virus into the cell (Takeda et al., 2003). After replication of virus in the cell, NA plays its major role in cleaving the terminal linkage between sialic acid and virus, releasing the progeny virions from the infected host cells. This cleavage will facilitate the virus to release and form sites of infection in the respiratory tract (McKimm-Breschkin, 2000). Due to its essential role in limiting the progression of influenza virus infection in the host and its relatively well-conserved active sites, NA has become an attractive target for structure-based antiviral drug development (An et al., 2009; Babu et al., 2000; Feng et al., 2013; Russell et al., 2006). So far, 17 subtypes of HA (H1-H17) and 10 subtypes of NA (N1-N10) circulating in avian and mammalian hosts have been identified (Tong et al., 2012; Von Itzstein, 2007). All known subtypes of influenza A viruses can infect

* Corresponding authors at: Institute of Functional Nano & Soft Materials (FUNSOM) and Jiangsu Key Laboratory for Carbon-Based Functional Materials & Devices, Soochow University, Suzhou, Jiangsu 215123, China.
E-mail addresses: lidancpu@outlook.com (D. Li), tingjunhou@hotmail.com, tingjunhou@zju.edu.cn (T. Hou).

0166-3542/$ - see front matter © 2013 Elsevier B.V. All rights reserved.
http://dx.doi.org/10.1016/j.antiviral.2013.09.006

birds, except for subtype H17N10 that has only been found in bats (Tong et al., 2012). Among the ten NA subtypes, only N1, N2 and N9 (i.e., H1N1, H3N2 and H7N9) have been found in human viruses responsible for pandemics and recurrent annual epidemics. When a new HA or NA subtype within a virus strain appears in the human population by genetic reassortment, it usually causes a pandemic because there is no preexisting immunity against the new virus.

Thus far, two types of drugs have been approved for clinical use against influenza virus. The first class is adamantanes (amantadine and rimantadine) (Dolin et al., 1982; Hay et al., 1985), which target the M2 proton channel of influenza (Pinto and Lamb, 2006). These drugs are not effective against influenza B (Pinto and Lamb, 2006; Stephenson and Nicholson, 1999), and some amantadine-resistant strains have also been reported (Monto and Arden, 1992). The second type is neuraminidase inhibitors (NAIs), including oseltamivir (OTV) and zanamivir (ZNV), which play vital roles in controlling influenza epidemics and pandemics (Moscona, 2005a). Different from adamantanes, both OTV and ZNV are effective against influenza A and B virus (Stephenson and Nicholson, 1999). Apart from OTV and ZNV, the cyclopentane analogue, peramivir (PRV) (Babu et al., 2000; Barroso et al., 2005), has also been tested with promising results. It has been approved in both Japan and South Korea and is currently in Phase III studies in the US. The chemical structures of the three NA inhibitors are shown in Fig. 1.

With the expanding use of these antiviral drugs, the possibility of mutations in NA, which can cause resistance to corresponding drugs, increases. In fact, several strains of the avian A/H5N1 (Le et al., 2005; Webster and Govorkova, 2006) and swine A/H1N1 influenza (Organization, 2009) have been found to cause resistance to OTV. For example, the OTV-resistant N294S and H274Y mutations in NA have been identified in the A/H3N2, A/H5N1, and A/H1N1 viruses (Collins et al., 2008; Gubareva et al., 2001; Kiso et al., 2004; Lackenby et al., 2008; Le et al., 2005). The resistance of NA to the available drugs, especially OTV, has been widely reported (McKimm-Breschkin, 2000; Moscona, 2005b). The emergence of the drug-resistant NAs for A/H1N1 indicates that the available drugs currently in use may not fully protect humans. Given the possible influenza pandemic caused by drug resistant strains and the restricted number of approved anti-influenza drugs, development of a new generation of anti-influenza drugs is of high priority. A clear understanding of the molecular mechanisms of drug resistance will certainly be beneficial for designing novel effective drugs against the resistant influenza strains.

In previous studies, molecular dynamics (MD) simulations and free energy calculations have been successfully applied to investigate drug-protein interactions in the catalytic site of NA and to identify novel druggable hot spots in the glycoprotein.(Amaro et al., 2007, 2011; Landon et al., 2008; Lawrenz et al., 2011; Masukawa et al., 2003; Rungrotmongkol et al., 2009; Udommaneethanakit et al., 2009) In addition, theoretical approaches have also been extensively used to expound the molecular mechanisms of the drug resistance of NA mutants. For example, in 2008, Malaisree et al., gave insights into the dynamic features of three NA inhibitors (OTV, ZNV and PRV) embedded in the active pocket of the N1 NA of the H5N1 avian virus, and their theoretical results given by the Molecular Mechanics/Poisson Boltzmann Surface Area (MM/PBSA) binding free energy calculations are in agreement with the experimental data for ranking the inhibitory activities.(Malaisree et al., 2008). In 2012, Woods et al., applied long-time scale MD simulations to figure out how the I223R/H275Y mutations in NA can lead to drug resistance and they observed that the binding affinity of OTV is significantly reduced because of the conformational changes that generate the open form of the 150-loop (Woods et al., 2012). Karthick et al., 2012 reported the influence of the H274Y mutation-induced OTV resistance in the H1N1 subtype NAs by molecular docking and MD simulations and found that the wild-type (WT) NA can be more indispensable for the OTV binding than the mutated NA, as characterized by the minimum number of H-bonds, high flexibility and largest binding affinity of the WT (Karthick et al., 2012).

The studies on the resistance mechanisms of A/H5N1 NA mutants have been extensively reported (Hitaoka et al., 2010; Nguyen et al., 2011; Park and Jo, 2009; Rungrotmongkol et al., 2009; Wang and Zheng, 2009). However, the resistance mechanisms of the 2009 A/H1N1 NA mutants to OTV, PRV and ZNV are not fully understood. Recently, we performed homology modeling, MD simulations and free energy calculations to reveal the drug resistance mechanisms of the H274Y, N294S and Y252H mutations in 2009 A/H1N1 NA to OTV (Li et al., 2012). In the current work, we intend to characterize the different sensitivities of OTV, PRV and ZNV against the WT and the E119G mutant of 2009 A/H1N1 NA (Fig. 2). The E119G mutation has been described in the viruses of the N2 subtype after serial passages in the presence of ZNV (Gubareva et al., 1997), and is responsible for the ZNV resistance in A/H3N2 and A/H5N1 viruses (Hurt et al., 2009; Mishin et al., 2005). It was also reported that the E119G mutant shows a PRV-resistance phenotype in the 2009 pandemic influenza A/H1N1 (pH1N1) background but interestingly remains susceptible to OTV (Pizzorno et al., 2011). To understand the different sensitivity of OTV, PRV and ZNV against the E119G mutant of 2009 A/H1N1 NA, MD simulations of the WT and E119G mutant bound with each inhibitor were first carried out. The binding free energy between each inhibitor and NA was then calculated using the Molecular Mechanics/Generalized Born Surface Area (MM/GBSA) method. Moreover, the MM/GBSA binding free energy decomposition analysis was applied to quantitatively characterize the contribution of each residue for the binding of the three inhibitors. By comparing the binding free energies and the structural features of the three inhibitors to the WT and mutated NAs, the mystery of the different sensitivities of OTV, PRV and ZNV against the E119G mutant of NA was comprehensively discussed.

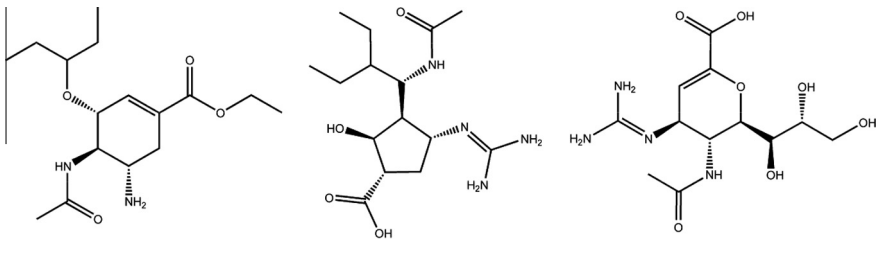

Fig. 1. Chemical structures of the three NA inhibitors: oseltamivir (OTV), zanamivir (ZNV), and peramivir (PRV).

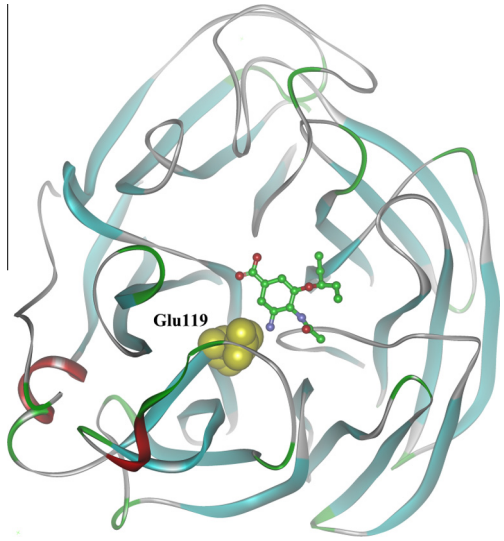

Fig. 2. Ribbon schematic representation of the 2009 Influenza A (H1N1) neuraminidase in complex with OTV. The position of the E119G mutation is highlighted in CPK model.

2. Materials and methods

2.1. Starting structures and protein preparation

The crystal structures of 2009 pandemic H1N1 NA in complex with OTV and ZNV (PDB entries: 3TI6 (Vavricka et al., 2011) and 3TI5 (Vavricka et al., 2011)) were retrieved from the RCSB Brookhaven Protein Data Bank. In order to generate the structure of the PRV–H1N1 complex, the structures of the PRV–N8 complex (PDB entry: 2HTU (Russell et al., 2006)) and the OTV–H1N1 complex (3TI6) were structurally aligned, and PRV was extracted from 2HTU and merged into 3TI6 to generate the corresponding structure of the PRV–H1N1 complex.

Because the X-ray crystal structures of the studied mutants are not available, the structures of the E119G mutants were generated by mutating their corresponding residues in the WT structures with the Discovery Studio 2.5 Guide and San Diego, 2009. Then, the six models (three WT and three drug-resistant mutants bound with OTV, PRV and ZNV) were used as the initial structures for the following MD simulations.

2.2. Molecular dynamics (MD) simulations

Each inhibitor was optimized and the electrostatic potential was calculated at the HF/6–31G* level using the Gaussian 09 program (Frisch et al., 2009). Subsequently, the atomic partial charges were obtained by a restraint electrostatic potential fit (RESP) method (Bayly et al., 1993). The partial charges and force field parameters for the inhibitors were generated automatically by the *antechamber* suite in AMBER11 (Case et al., 2005). The general AMBER force field (*gaff*) (Wang et al., 2004) was used for the inhibitors, and AMBER ff12SB force field (Case et al., 2012) for the proteins. All missing hydrogen atoms of the proteins were added using the *leap* module in AMBER11 (Case et al., 2005). There are eight disulfide bonds in the protein and they were properly enforced using the CYX notation. Protonation states for the histidine residues were determined at pH = 6.5 using the PDB2PQR web server (Dolinsky et al., 2007). Four counter ions of Cl^- were placed to neutralize the charge of the system. Each system was then immersed into a rectangular box of the TIP3P (Jorgensen et al., 1983) water molecules, with a distance of 10 Å extended from any solute atom. Particle Mesh Ewald (PME) algorithm (Darden et al., 1993) was applied to handle the long-range electrostatics in a periodic boundary condition.

Before the MD simulations, each system was subjected to three-stage minimizations by the *sander* program in AMBER11 (Case et al., 2005). In the first stage, 1000 cycles of minimization (500 cycles of steepest descent and 500 cycles of conjugate gradient minimization) were carried out with the backbone carbons constrained (50 kcal/mol/Å^2). Then, 1000 cycles of minimization with relatively weaker constraint (10 kcal/mol/Å^2) were conducted. Finally, 5000 cycles (1000 cycles of steepest descent and 4000 cycles of conjugate gradient minimization) of full energy minimization without any constraint were carried out. After minimization, each system was gradually heated from 0 to 300 K over a period of 50 ps with 2.0 kcal/mol/Å^2 restraints on the complex, and then another 50 ps NPT MD simulations were followed at 300 K. Subsequently, the MD simulations with a target temperature of 300 K and a target pressure of 1 atm were performed. The SHAKE algorithm was applied to constrain all bonds involving hydrogen atoms (Ryckaert et al., 1977), and the time step was set to 2.0 fs. Coordinates were saved every 10 ps during the MD runs.

2.3. MM/GBSA binding free energy calculations

The binding free energy for each system was calculated by the MM/GBSA approach (Kollman et al., 2000; Wang et al., 2006), which integrates both molecular mechanics and continuum solvent model (Gohlke et al., 2003; Huo et al., 2002a, 2002b; Hou et al., 2003, 2008a, 2009, 2011; Hou and Yu, 2007; Kuhn et al., 2005; Kuhn and Kollman, 2000; Li et al., 2012; Liu et al., 2010; Xu et al., 2013; Xue et al., 2012; Yang et al., 2011; Zhang et al., 2010). The binding free energy (ΔG_{bind}) of the inhibitor in each complex was calculated according to Eq. (1). In the MM/GBSA calculations, the single-trajectory protocol, which has higher stability of prediction than the separate-trajectory protocol, was used (Hou and Yu, 2007; Wang et al., 2006***).

$$\begin{aligned} \Delta G_{bind} &= G_{complex} - G_{protein} - G_{ligand} = \Delta H + \Delta G_{solvation} - T\Delta S \\ &= \Delta E_{MM} + \Delta G_{GB} + \Delta G_{SA} - T\Delta S \quad (1) \end{aligned}$$

where ΔE_{MM} is the gas-phase interaction energy between protein and ligand, including the electrostatic and van der Waals interactions; ΔG_{GB} and ΔG_{SA} are the polar and non-polar components of the desolvation free energy, respectively; $-T\Delta S$ is the change of the conformational entropy upon ligand binding, which was not considered here due to the very high computational cost and low prediction accuracy (Hou et al., 2011; Wang et al., 2006). The polar contribution of desolvation (ΔG_{GB}) was calculated using the generalized Born (GB) model with the parameters developed by Onufriev et al. (*igb* = 2) (Onufriev et al., 2000). The exterior dielectric constant was set to 80, and the solute dielectric constant was set to 2. The non-polar contribution (ΔG_{SA}) to desolvation was estimated by the solvent-accessible surface area (SASA) based on the LCPO method (Weiser et al., 1999): $\Delta G_{\text{SA}} = 0.0072 \times \Delta\text{SASA}$.

2.4. MM/GBSA binding free energy decomposition

For each complex, the protein-inhibitor interaction spectrum on a per-residue basis was computed by the MM/GBSA free energy decomposition analysis supported in the *mm_pbsa* program of AMBER11 (Hou et al., 2008b, 2009, 2012). The residue-inhibitor interactions have four components as shown in Eq. (2):

$$\Delta G_{inhibitor-residue} = \Delta E_{vdw} + \Delta G_{ele} + \Delta G_{GB} + \Delta G_{SA} \quad (2)$$

where ΔE_{vdw} and ΔE_{ele} represent van der Waals and electrostatic contributions to inhibitor-residue interactions; ΔG_{GB} and ΔG_{SA} rep-

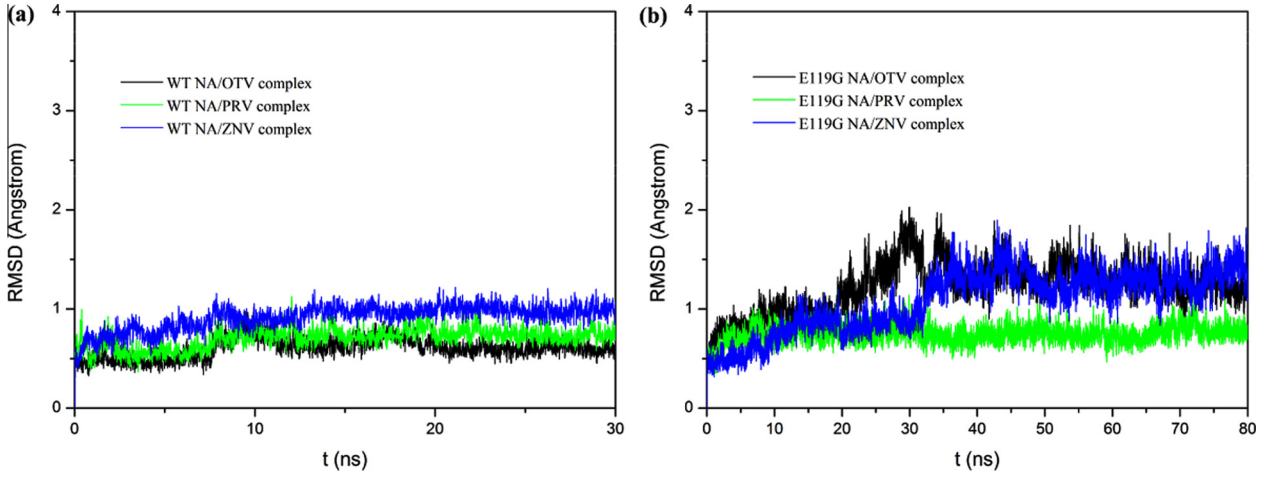

Fig. 3. Time evolution of the root-mean-square displacements (RMSDs) of the residues within 5 Å around the ligand. (a) The WT NA in complex with OTV, PRV and ZNV (black: the WT/OTV complex, green: the WT/PRV complex, blue: the WT/ZNV complex); (b) the E119G NA in complex with OTV, PRV and ZNV (black: the E119G/OTV complex, green: the E119G/PRV complex, blue: the E119G/ZNV complex). (For interpretation of the references to color in this figure legend, the reader is referred to the web version of this article.)

resent polar and non-polar contributions of desolvation to inhibitor-residue interactions. ΔG_{GB} was calculated by the GB model with the parameters developed by Onufriev et al. (*igb* = 2) (Onufriev et al., 2000), and ΔG_{SA} was computed by SASA using the ICOSA technique (Gohlke et al., 2003). The exterior dielectric constant was set to 80, and the solute dielectric constant was set to 2.

3. Results and discussion

3.1. Simulation stability of the WT and mutated complexes

To evaluate the structural stability of the dynamic trajectories, the root-mean-square displacements (RMSDs) of the residues within 5 Å around ligand for each complex are illustrated in Fig. 3. For all systems, 30 ns MD simulations were first carried out to produce the trajectories. However, for the three E119G mutants, extra 50 ns MD simulations were performed. From the time evolution of RMSDs of the WT and mutated complexes, we can observe that the WT complexes almost reach equilibration in 10 ns, which are much faster than the mutated complexes. This phenomenon can be explained by the change of the interactions between the mutated residue and the surrounding residues, which might introduce perturbation to the original structure and therefore longer simulations are necessary to stabilize the mutated systems. Moreover, it can be observed that the RMSDs of the mutants, especially the E119G/OTV and E119G/ZNV complexes, are relatively higher than that of the WT complexes, which indicates that the mutated systems drift further away from the original structures.

3.2. Assessment of the different sensitivities of OTV, PRV and ZNV against the E119G NA mutant by MM/GBSA predictions

MM/GBSA was well known as a successful method to compare the binding affinities of closely related inhibitors in closely related binding pockets and to gain rational insights into their differences of binding. Here, the sensitivity of each inhibitor against the E119G mutant was quantitatively evaluated by the MM/GBSA binding free energy between NA and each inhibitor. The binding affinities (ΔG_{Bind}) and the energetic components predicted by MM/GBSA for the WT complexes based on the 20–30 ns MD trajectories and the three mutants based on the 50–80 ns MD trajectories are summarized in Table 1. According to our calculations, the predicted binding free energies of OTV, PRV and ZNV bound with the E119G mutant are −24.40, −34.48 and −20.02 kcal/mol, respectively, which are all higher than those of the WT complexes (−25.63, −36.31 and −28.79 kcal/mol, respectively). The drop of the binding affinities of OTV, PRV and ZNV indicates that the E119G mutation in NA confers resistance to all the three inhibitors. However, the sensitivities of OTV, PRV and ZNV against the E119G mutant are different. The rank of the resistance level predicted by the ΔG_{Bind} values for the three inhibitors is: ZNV > PRV > OTV. It is encouraging that the predictions are well consistent with the experimental data, where ZNV shows the highest level of resistance (832-fold) and OTV exhibits relatively retained susceptibility to the E119G mutated NA (2.9-fold).

According to the energetic components of the binding free energies presented in Table 1, one can observe that the van der Waals (ΔE_{vdw}), non-polar desolvation (ΔG_{SA}) and electrostatic (ΔE_{ele})

Table 1
The energetic components of the predicted binding free energies between inhibitor and NA (ε_{in} = 2.0).

Energy	WT/OTV	E119G/OTV	WT/PRV	E119G/PRV	WT/ZNV	E119G/ZNV
ΔE_{vdw}	−26.65 ± 0.21	−25.70 ± 0.20	−29.71 ± 0.78	−31.66 ± 0.11	−26.46 ± 0.15	−25.89 ± 0.80
ΔG_{SA}	−2.90 ± 0.01	−2.84 ± 0.05	−3.61 ± 0.09	−3.73 ± 0.01	−3.07 ± 0.04	−2.86 ± 0.02
ΔE_{ele}	−20.77 ± 0.89	−14.95 ± 1.06	−35.16 ± 1.07	−30.80 ± 0.04	−45.72 ± 0.23	−18.72 ± 3.20
ΔG_{GB}	24.69 ± 0.56	19.09 ± 0.36	32.17 ± 1.64	31.72 ± 0.07	46.45 ± 0.39	27.46 ± 1.90
ΔG_{Bind}[a]	−25.63 ± 0.12	−24.40 ± 0.95	−36.31 ± 1.44	−34.48 ± 0.22	−28.79 ± 0.04	−20.02 ± 0.46
IC_{50}, nM (Ratio)[b]	0.46 (1)	1.34 (2.9)	0.09 (1)	4.61 (51.2)	0.15 (1)	124.9 (832)

[a] Standard deviations based on two blocks.
[b] Compared with that of the WT virus.

terms are favorable to ligand binding for all systems, whereas the polar desolvation term (ΔG_{GB}) is unfavorable. The van der Waals (ΔE_{vdw}) contributions for the binding of OTV, PRV or ZNV to the E119G mutants (−25.70, −31.66 and −25.89 kcal/mol, respectively) change slightly compared with those to the corresponding WT proteins (−26.65, −29.71 and −26.46 kcal/mol, respectively). Moreover, due to little variations of the non-polar desolvation (ΔG_{SA}) terms among different systems, the total non-polar interactions ($\Delta E_{vdw} + \Delta G_{SA}$) of all the three inhibitors are stable upon the E119G mutation in NA. However, the favorable electrostatic (ΔE_{ele}) interaction and the unfavorable polar desolvation (ΔG_{GB}) interaction between the E119G mutant and each inhibitor are significantly weakened compared with that between WT and each inhibitor. Though we should notice that the total polar contribution ($\Delta E_{ele} + \Delta G_{GB}$) of the E119G/OTV complex is only slightly influenced compared with that of the WT/OTV complex (from 3.92 to 4.14 kcal/mol). For the PRV (from −2.99 to 0.92 kcal/mol) and ZNV (from 0.73 to 8.74 kcal/mol) systems, the impacts of the total polar contributions is more significant. Furthermore, the rank of the changes of the polar contributions for the three inhibitors caused by the E119G mutation (ZNV > PRV > OTV) is in good agreement with the ordering of drug resistance. Our findings indicate that the polar interactions determinate the different sensitivities of OTV, PRV and ZNV against the E119G mutants of NA.

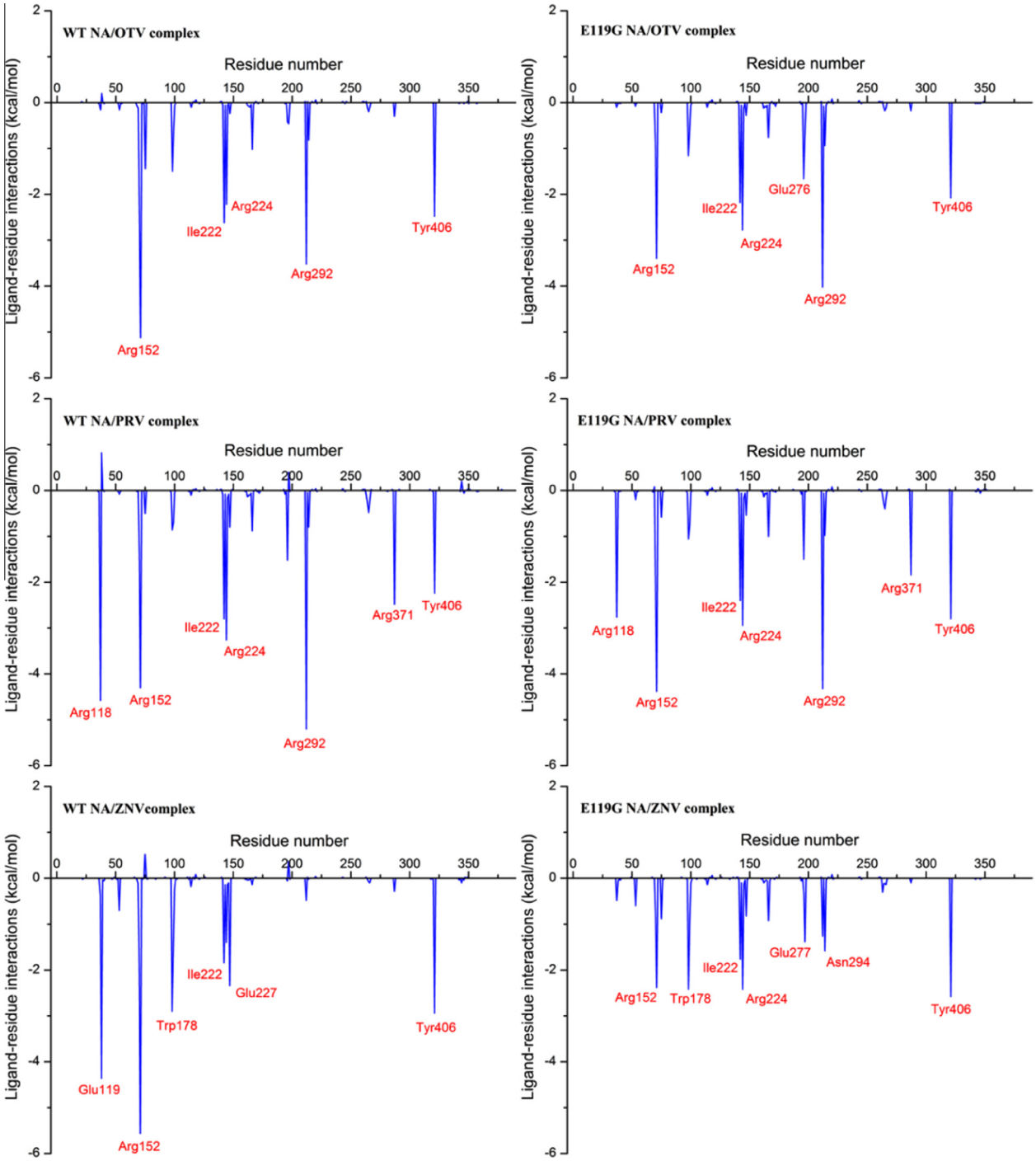

Fig. 4. The protein-inhibitor interaction spectra of the WT and E119G mutants in complex with OTV, PRV and ZNV.

3.3. Susceptibility of OTV, PRV and ZNV over the E119G mutation in NA

In order to uncover the binding modes of OTV, PRV and ZNV and reveal the resistance mechanisms of the inhibitors caused by the E119G mutation at the atomic level, the protein-inhibitor interaction spectrum on a per-residue basis for each inhibitor bound with WT or E119G mutant was generated by the MM/GBSA free energy decomposition analysis and plotted in Fig. 4.

3.3.1. The resistance mechanism of OTV against the E119G mutation

Glu119 is an active site residue that can form direct contact with OTV. Strong H-bonds between the carboxyl oxygen atoms of Glu119 and the amino hydrogen of OTV are formed. The E119G mutation belongs to the replacement of a larger group with a smaller glycine group. It is reasonable to suppose that this alteration would significantly influence the binding affinity of OTV due to the removal of the carboxymethyl group, which directly causes the missing of the interactions between the residue 1119 and OTV. However, regarding the results from the experiments (Pizzorno et al., 2011), the binding affinity of OTV is only slightly decreased when Glu119 is mutated to Gly (2.9-fold). To reveal the influence of the E119G mutation on the binding of OTV and the corresponding resistance mechanism, the averaged structure of the E119G/OTV complex generated from the last 30 ns MD trajectories was superimposed to that of the WT/OTV system from the last 10 ns trajectories (Fig. 5a), and the energetic components of the important residues are also listed in Table S1 in the Supporting Information. As we can see from Fig. 5a, OTV can form several H-bonds with the residue Glu119, Arg152 and Arg292. According to the energy decomposition analysis (Fig. 4), the essential residues for the binding of OTV to the WT NA are Arg152, Ile222, Arg224, Arg292 and Tyr406. It is interesting to observe that the residue Glu119 almost has no energetic contribution to the binding of OTV to the WT NA. The detailed energetic components in Table S1 show that the electrostatic (ΔE_{ele}) interactions between Glu119 and OTV are strong (−5.46 kcal/mol), whereas the polar desolvation (ΔG_{GB}) interactions are more unfavorable (7.20 kcal/mol), which makes the total energetic contributions of Glu119 negligible. Therefore, the impact of E119G mutation on the binding of OTV is quite limited. The structural superimposition of the WT/OTV and E119G/OTV complexes reveals that the conformation of OTV only slightly changes upon the E119G mutation (RMSD = 1.6337 Å), and most residues in the binding pocket of the two systems are well aligned. The most significant energetic reduction is found for the residue Arg152, whose contribution changes from −5.12 to −3.40 kcal/mol. It is noticeable that the H-bond between Arg152 and OTV still remains, but the length of the H-bond in the E119G complex (1.778 Å) is longer than that in the WT complex (1.705 Å), which results in the decrease of the polar contributions of Arg152 to the OTV binding.

3.3.2. The resistance mechanism of PRV against the E119G mutation

Previous study showed that the E119G mutation confers resistance to PRV with 51-fold increase of the IC_{50} values. As we can see from Fig. 5b, strong H-bonds of PRV with the residues Glu119, Arg152, Arg292 and Arg371 in the WT NA can be monitored. Though no H-bond is formed between PRV and the residue Arg118, the polar interactions between them are quite strong. In addition to the contributions of these polar residue side chains, the residues Ile222 and Tyr406, which are non-polar residues, also have obvious contributions to the PRV binding owing to their relatively strong non-polar interactions with PRV. According to the detailed energetic components of these residues in Table S2, it is discovered that the residue Glu119 in the WT complex is slimly unfavorable to the PRV binding. This phenomenon is similar to the situation of Glu119 to the OTV binding, where the unfavorable polar desolvation (ΔG_{GB}) contribution plays the leading role. A close-up view of the structural superimposition of the WT/PRV and E119G/PRV complexes demonstrates that most binding site

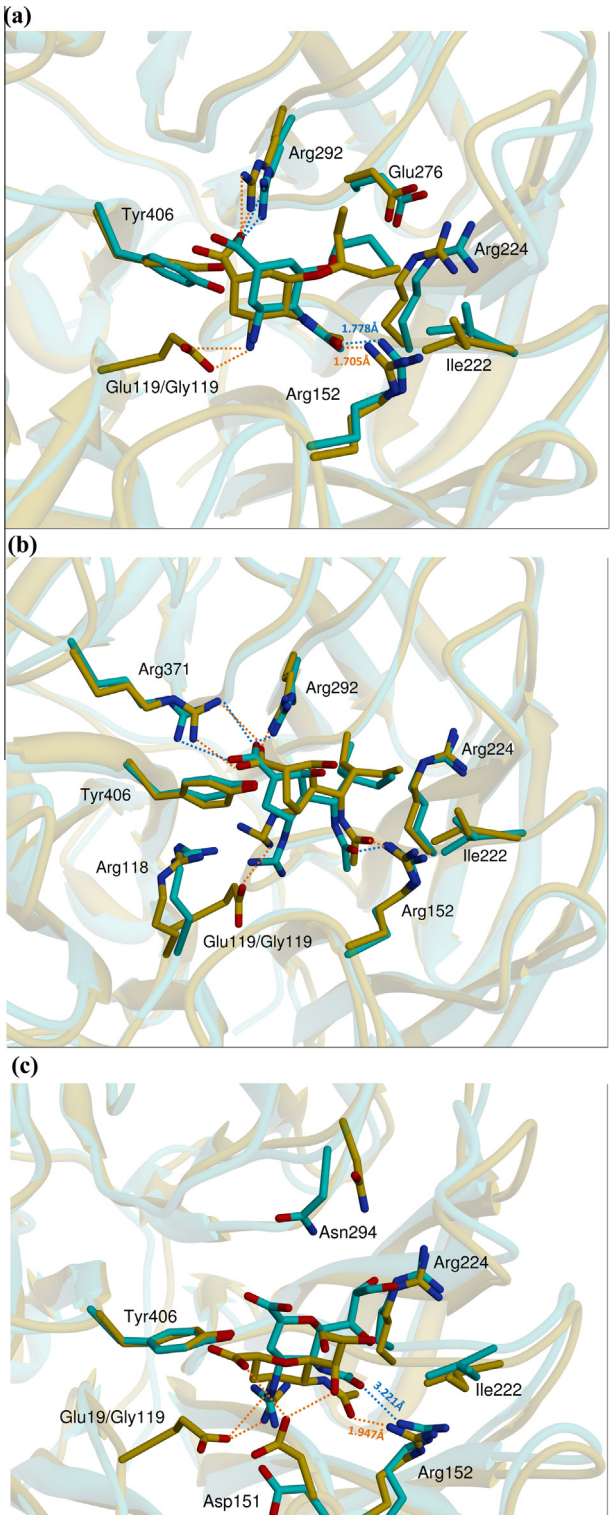

Fig. 5. The structural superimposition and schematic representation of the interactions for (a) the WT/OTV complex (yellow) and the E119G/OTV complex (cyan); (b) the WT/PRV complex (yellow) and the E119G/PRV complex (cyan); (c) the WT/ZNV complex (yellow) and the E119G/ZNV complex. All structures are averaged conformations generated from the stable trajectories. The H-bonds of the WT complexes are labeled with the yellow dotted lines and those of the E119G mutant complexes are labeled with the cyan ones. (For interpretation of the references to color in this figure legend, the reader is referred to the web version of this article.)

residues do not have huge conformational change upon the E119G mutation, and most H-bonds found in the WT complex are still maintained. The RMSDs of PRV between WT and E119G mutant are 0.9245 Å, which indicates that the variation of PRV upon E119G mutation is small. However, significant slide of the guanidine group of PRV is observed. This conformational change directly affects the strong polar interactions between Arg118 and PRV (from −5.62 to −2.10 kcal/mol). The decrease of the energetic contributions of Arg118 is responsible for the development of drug resistance of PRV against the E119G NA. In addition, several residues, such as Arg292, Arg371 and Tyr406, are also influenced by the E119G mutation, but the variations of the energetic contributions of these residues are limited.

3.3.3. The resistance mechanism of ZNV against the E119G mutation

ZNV exhibits the highest level of drug resistance among the three studied inhibitors with 830-fold increase of the IC_{50} values. As we discussed above, the trend of the binding free energies of ZNV is well consistent with the experimental data. The protein-inhibitor interaction spectra are plotted in Fig. 4 with the key residues highlighted. It is observed that the dominating interactions between ZNV and the WT NA are the bindings to the side chains of Glu119, Asp151, Arg152, Trp178, Ile222, Glu227 and Tyr406. Among them, the residues Glu119, Asp151 and Arg152 can form strong H-bonds with ZNV. Different from the situation of Glu119 for the binding of OTV and PRV, the residue Glu119 plays an important role in the binding of ZNV to the WT NA, where the total energetic contribution of Glu119 is −4.36 kcal/mol. When Glu119 is mutated to a smaller glycine group, the energetic contribution of Gly119 almost falls to zero due to the loss of the strong interactions between Glu119 and ZNV. Moreover, the geometry of ZNV is significantly shifted from the original state in the WT complex (RMSD = 2.7197 Å), which indirectly affects the binding of the surrounding residues. As displayed in Fig. 5c, ZNV moves closer to the residues Arg224 and Asn294 along with an obvious rotation in the structure itself. This variation leads to the rearrangement of the energy distribution of the binding site residues. As shown in Fig. 4, almost all the residues that play key roles in the binding of ZNV to the WT NA are affected and their energetic contributions are significantly reduced. We can find that the H-bonds between Asp151 and ZNV are disrupted by the conformational change of ZNV, and the one between Arg152 and ZNV is also strongly weakened since the length of the H-bond changes from 1.947 Å to 3.221 Å. This observation is also supported by the energy decomposition results listed in Table S3, where the favorable electrostatic (ΔE_{ele}) contributions of both Asp151 and Arg152 are prominently diminished. In addition, some residues, such as Arg224, Glu277 and Asn294, emerge as new energy contributors to the binding of ZNV, but this cannot make up for the loss of the energies produced by other residues.

4. Conclusions

In this study, a sequence of molecular modeling techniques, including MD simulations, MM/GBSA binding free energy calculations, and MM/GBSA binding free energy decomposition analysis, were applied to reveal the mystery of the different sensitivities of OTV, PRV and ZNV against the E119G mutant of 2009 A/H1N1 NA. The order of the resistance level predicted by the MM/GBSA binding free energy calculations for the three inhibitors (ZNV > PRV > OTV) is in good agreement with the experimental data, where ZNV shows the highest level of resistance (832-fold) and OTV exhibits relatively retained susceptibility to the E119G mutant (2.9-fold).

According to the analyses of the energetic components for each system, we observe that the variations of the polar interactions play key roles in the emergency of the drug resistance for all the three studied inhibitors and at the same time determinate the different sensitivities of OTV, PRV and ZNV against the E119G mutant of NA. For both OTV and PRV, the energetic contributions of the residue 119 which can form H-bonds with the inhibitors in the WT NA do not change much upon the E119G mutation due to the impact of the strong unfavorable polar desolvation interactions. The limited drug resistance of OTV is mainly caused by the small variation of the residue Arg152. For PRV, the conformational change of the guanidine scaffold directly affects the polar interactions between Arg118 and PRV, which are responsible for the development of the drug resistance to PRV caused by E119G mutation. Among the three studied inhibitors, ZNV shows the highest level of drug resistance. Significant change of the geometry of ZNV is observed upon the E119G mutation compared with that in the WT system, and several H-bonds with Asp151 and Arg152 formed in the WT complex are also disrupted. In order to minimize the impact of the E119G mutation on the binding of NA inhibitors, future drug design could consider the reduction of the interactions between inhibitor and the residue Glu119 since more H-bonds do not always give rise to a much stronger binding affinity but possibly make the inhibitor more sensitivity to the mutation. As the case in this study, OTV exhibits the lowest level of drug resistance to the E119G mutation because of the relatively smaller amino-group in OTV that interacts with Glu119. The structural analysis and quantitative viewpoint from this work disclose the mechanisms of the different sensitivities of OTV, PRV and ZNV against the E119G mutant of NA and provide helpful information for the rational design of new and effective drugs to combat drug resistance.

Acknowledgment

This study was supported by the National Science Foundation of China (21173156), the National Basic Research Program of China (973 program, 2012CB932600), and the Priority Academic Program Development of Jiangsu Higher Education Institutions (PAPD).

Appendix A. Supplementary data

Supplementary data associated with this article can be found, in the online version, at http://dx.doi.org/10.1016/j.antiviral.2013.09.006.

References

Amaro, R.E., Minh, D.D.L., Cheng, L.S., Lindstrom Jr, W.M., Olson, A.J., Lin, J.H., Li, W.W., McCammon, J.A., 2007. Remarkable loop flexibility in avian influenza N1 and its implications for antiviral drug design. J. Am. Chem. Soc. 129, 7764–7765.

Amaro, R.E., Swift, R.V., Votapka, L., Li, W.W., Walker, R.C., Bush, R.M., 2011. Mechanism of 150-cavity formation in influenza neuraminidase. Nat. Commun. 2, 388.

An, J., Lee, D.C.W., Law, A.H.Y., Yang, C.L.H., Poon, L.L.M., Lau, A.S.Y., Jones, S.J.M., 2009. A novel small-molecule inhibitor of the avian influenza H5N1 virus determined through computational screening against the neuraminidase. J. Med. Chem. 52, 2667–2672.

Arias, C.F., Escalera-Zamudio, M., de los Dolores Soto-Del Río, M., Georgina Cobián-Güemes, A., Isa, P., López, S., 2009. Molecular anatomy of 2009 influenza virus A (H1N1). Arch. Med. Res. 40, 643–654.

Babu, Y.S., Chand, P., Bantia, S., Kotian, P., Dehghani, A., El-Kattan, Y., Lin, T.-H., Hutchison, T.L., Elliott, A.J., Parker, C.D., 2000. BCX-1812 (RWJ-270201): discovery of a novel, highly potent, orally active, and selective influenza neuraminidase inhibitor through structure-based drug design. J. Med. Chem. 43, 3482–3486.

Barroso, L., Treanor, J., Gubareva, L., Hayden, F.G., 2005. Efficacy and tolerability of the oral neuraminidase inhibitor peramivir in experimental human influenza: randomized, controlled trials for prophylaxis and treatment. Antiviral Ther. 10, 901.

Bayly, C.I., Cieplak, P., Cornell, W., Kollman, P.A., 1993. A well-behaved electrostatic potential based method using charge restraints for deriving atomic charges: the RESP model. J. Phys. Chem. 97, 10269–10280.
Case, D.A., Cheatham, T.E., Darden, T., Gohlke, H., Luo, R., Merz, K.M., Onufriev, A., Simmerling, C., Wang, B., Woods, R.J., 2005. The Amber biomolecular simulation programs. J. Comput. Chem. 26, 1668–1688.
Case, D.A., Darden, T.A., Cheatham III, T.E., Simmerling, C.L., Wang, J., Duke, R.E., Luo, R., Walker, R.C., Zhang, W., Merz, K.M., 2012. AMBER, 12th ed. University of California, San Francisco, San Francisco.
Collins, P.J., Haire, L.F., Lin, Y.P., Liu, J., Russell, R.J., Walker, P.A., Skehel, J.J., Martin, S.R., Hay, A.J., Gamblin, S.J., 2008. Crystal structures of oseltamivir-resistant influenza virus neuraminidase mutants. Nature 453, 1258–1261.
Darden, T., York, D., Pedersen, L., 1993. Particle mesh Ewald: an W log (N) method for Ewald sums in large systems. J. Chem. Phys. 98, 10089–10092.
Discovery Studio 2.5 Guide, Accelrys Inc., San Diego, 2009. Available from: http://www.accelrys.com.
Dolin, R., Reichman, R.C., Madore, H.P., Maynard, R., Linton, P.N., Webber-Jones, J., 1982. A controlled trial of amantadine and rimantadine in the prophylaxis of influenza A infection. N. Engl. J. Med. 307, 580–584.
Dolinsky, T.J., Czodrowski, P., Li, H., Nielsen, J.E., Jensen, J.H., Klebe, G., Baker, N.A., 2007. PDB2PQR: expanding and upgrading automated preparation of biomolecular structures for molecular simulations. Nucleic Acids Res. 35, W522–W525.
Feng, E., Shin, W.-J., Zhu, X., Li, J., Ye, D., Wang, J., Zheng, M., Zuo, J.-P., No, K.T., Liu, X., Zhu, W., Tang, W., Seong, B.-L., Jiang, H., Liu, H., 2013. Structure-based design and synthesis of C-1- and C-4-modified analogs of zanamivir as neuraminidase inhibitors. J. Med. Chem. 56, 671–684.
Ferguson, N.M., Fraser, C., Donnelly, C.A., Ghani, A.C., Anderson, R.M., 2004. Public health risk from the avian H5N1 influenza epidemic. Science 304, 968–969.
Frisch, M.J., Trucks, G., Schlegel, H., Scuseria, G., Robb, M., Cheeseman, J., Scalmani, G., Barone, V., Mennucci, B., Petersson, G., 2009. Gaussian 09. Gaussian. Inc., Wallingford, CT.
Garten, R.J., Davis, C.T., Russell, C.A., Shu, B., Lindstrom, S., Balish, A., Sessions, W.M., Xu, X., Skepner, E., Deyde, V., 2009. Antigenic and genetic characteristics of swine-origin 2009 A (H1N1) influenza viruses circulating in humans. Science 325, 197–201.
Gohlke, H., Kiel, C., Case, D.A., 2003. Insights into protein-protein binding by binding free energy calculation and free energy decomposition for the Ras–Raf and Ras–RalGDS complexes. J. Mol. Biol. 330, 891–913.
Gubareva, L.V., Robinson, M.J., Bethell, R.C., Webster, R.G., 1997. Catalytic and framework mutations in the neuraminidase active site of influenza viruses that are resistant to 4-guanidino-Neu5Ac2en. J. Virol. 71, 3385–3390.
Gubareva, L.V., Kaiser, L., Matrosovich, M.N., Soo-Hoo, Y., Hayden, F.G., 2001. Selection of influenza virus mutants in experimentally infected volunteers treated with oseltamivir. J. Infect. Dis. 183, 523–531.
Hay, A., Wolstenholme, A., Skehel, J., Smith, M.H., 1985. The molecular basis of the specific anti-influenza action of amantadine. EMBO J. 4, 3021.
Hitaoka, S., Harada, M., Yoshida, T., Chuman, H., 2010. Correlation analyses on binding affinity of sialic acid analogues with influenza virus neuraminidase-1 using ab initio MO calculations on their complex structures. J. Chem. Inf. Model. 50, 1796–1805.
Hou, T., Yu, R., 2007. Molecular dynamics and free energy studies on the wild-type and double mutant HIV-1 protease complexed with amprenavir and two amprenavir-related inhibitors: mechanism for binding and drug resistance. J. Med. Chem. 50, 1177–1188.
Hou, T.J., Zhu, L.L., Chen, L.R., Xu, X.J., 2003. Mapping the binding site of a large set of quinazoline type EGF-R inhibitors using molecular field analyses and molecular docking studies. J. Chem. Inf. Comp. Sci. 43, 273–287.
Hou, T., McLaughlin, W.A., Wang, W., 2008a. Evaluating the potency of HIV-1 protease drugs to combat resistance. Proteins: Struct., Funct., Bioinf. 71, 1163–1174.
Hou, T., Zhang, W., Case, D.A., Wang, W., 2008b. Characterization of domain-peptide interaction interface. A case study on the amphiphysin-1 SH3 domain. J. Mol. Biol. 376, 1201–1214.
Hou, T.J., Xu, Z., Zhang, W., McLaughlin, W.A., Case, D.A., Xu, Y., Wang, W., 2009. Characterization of domain-peptide interaction interface. Mol. Cell. Proteomics 8, 639–649.
Hou, T., Wang, J., Li, Y., Wang, W., 2011. Assessing the performance of the MM/PBSA and MM/GBSA methods. 1. the accuracy of binding free energy calculations based on molecular dynamics simulations. J. Chem. Inf. Model. 51, 69–82.
Hou, T., Li, N., Li, Y., Wang, W., 2012. Characterization of domain-peptide interaction interface: prediction of SH3 domain-mediated protein–protein interaction network in yeast by generic structure-based models. J. Proteome Res. 11, 2982.
Hsieh, Y.C., Wu, T.Z., Liu, D.P., Shao, P.L., Chang, L.Y., Lu, C.Y., Lee, C.Y., Huang, F.Y., Huang, L.M., 2006. Influenza pandemics: past, present and future. J. Formos. Med. Assoc. 105, 1–6.
Huo, S., Massova, I., Kollman, P.A., 2002a. Computational alanine scanning of the 1:1 human growth hormone–receptor complex. J. Comput. Chem. 23, 15–27.
Huo, S., Wang, J., Cieplak, P., Kollman, P.A., Kuntz, I.D., 2002b. Molecular dynamics and free energy analyses of cathepsin D-inhibitor interactions: insight into structure-based ligand design. J. Med. Chem. 45, 1412–1419.
Hurt, A.C., Holien, J.K., Barr, I.G., 2009. In vitro generation of neuraminidase inhibitor resistance in A (H5N1) influenza viruses. Antimicrob. Agents Chemother. 53, 4433–4440.
Jorgensen, W.L., Chandrasekhar, J., Madura, J.D., Impey, R.W., Klein, M.L., 1983. Comparison of simple potential functions for simulating liquid water. J. Chem. Phys. 79, 926.
Karthick, V., Shanthi, V., Rajasekaran, R., Ramanathan, K., 2012. Exploring the cause of oseltamivir resistance against mutant H274Y neuraminidase by molecular simulation approach. Appl. Biochem. Biotechnol., 1–13.
Kiso, M., Mitamura, K., Sakai-Tagawa, Y., Shiraishi, K., Kawakami, C., Kimura, K., Hayden, F.G., Sugaya, N., Kawaoka, Y., 2004. Resistant influenza A viruses in children treated with oseltamivir: descriptive study. The Lancet 364, 759–765.
Kollman, P.A., Massova, I., Reyes, C., Kuhn, B., Huo, S., Chong, L., Lee, M., Lee, T., Duan, Y., Wang, W., 2000. Calculating structures and free energies of complex molecules: combining molecular mechanics and continuum models. Acc. Chem. Res. 33, 889–897.
Kuhn, B., Kollman, P.A., 2000. Binding of a diverse set of ligands to avidin and streptavidin: An accurate quantitative prediction of their relative affinities by a combination of molecular mechanics and continuum solvent models. J. Med. Chem. 43, 3786–3791.
Kuhn, B., Gerber, P., Schulz-Gasch, T., Stahl, M., 2005. Validation and use of the MM-PBSA approach for drug discovery. J. Med. Chem. 48, 4040–4048.
Lackenby, A., Hungnes, O., Dudman, S., Meijer, A., Paget, W., Hay, A., Zambon, M., 2008. Emergence of resistance to oseltamivir among influenza A (H1N1) viruses in Europe. Euro Surveill., 13.
Landon, M.R., Amaro, R.E., Baron, R., Ngan, C.H., Ozonoff, D., Andrew McCammon, J., Vajda, S., 2008. Novel druggable hot spots in avian influenza neuraminidase H5N1 revealed by computational solvent mapping of a reduced and representative receptor ensemble. Chem. Biol. Drug Des. 71, 106–116.
Lawrenz, M., Baron, R., Wang, Y., McCammon, J.A., 2011. Effects of biomolecular flexibility on alchemical calculations of absolute binding free energies. J. Chem. Theory Comput. 7, 2224–2232.
Le, Q.M., Kiso, M., Someya, K., Sakai, Y.T., Nguyen, T.H., Nguyen, K.H.L., Pham, N.D., Ngyen, H.H., Yamada, S., Muramoto, Y., 2005. Avian flu: isolation of drug-resistant H5N1 virus. Nature 437, 1108.
Li, L., Li, Y., Zhang, L., Hou, T., 2012. Theoretical studies on the susceptibility of oseltamivir against variants of 2009 A/H1N1 influenza neuraminidase. J. Chem. Inf. Model. 52, 2715–2729.
Liu, H., Yao, X., Wang, C., Han, J., 2010. In silico identification of the potential drug resistance sites over 2009 influenza A (H1N1) virus neuraminidase. Mol. Pharm. 7, 894–904.
Malaisree, M., Rungrotmongkol, T., Decha, P., Intharathep, P., Aruksakunwong, O., Hannongbua, S., 2008. Understanding of known drug-target interactions in the catalytic pocket of neuraminidase subtype N1. Proteins: Struct., Funct., Bioinf. 71, 1908–1918.
Masukawa, K.M., Kollman, P.A., Kuntz, I.D., 2003. Investigation of neuraminidase-substrate recognition using molecular dynamics and free energy calculations. J. Med. Chem. 46, 5628–5637.
McKimm-Breschkin, J.L., 2000. Resistance of influenza viruses to neuraminidase inhibitors—a review. Antiviral Res. 47, 1–17.
Mishin, V.P., Hayden, F.G., Gubareva, L.V., 2005. Susceptibilities of antiviral-resistant influenza viruses to novel neuraminidase inhibitors. Antimicrob. Agents Chemother. 49, 4515–4520.
Monto, A.S., Arden, N.H., 1992. Implications of viral resistance to amantadine in control of influenza A. Clin. Infect. Dis. 15, 362–367.
Moscona, A., 2005a. Neuraminidase inhibitors for influenza. N. Engl. J. Med. 353, 1363–1373.
Moscona, A., 2005b. Oseltamivir resistance—disabling our influenza defenses. N. Engl. J. Med. 353, 2633–2636.
Neumann, G., Noda, T., Kawaoka, Y., 2009. Emergence and pandemic potential of swine-origin H1N1 influenza virus. Nature 459, 931–939.
Nguyen, T.T., Mai, B.K., Li, M.S., 2011. Study of Tamiflu sensitivity to variants of A/H5N1 virus using different force fields. J. Chem. Inf. Model. 51, 2266–2276.
Onufriev, A., Bashford, D., David, A., 2000. Modification of the generalized Born model suitable for macromolecules. J. Phys. Chem. 104, 3712–3720.
Organization, W.H., 1980. A revision of the system of nomenclature for influenza viruses: a WHO memorandum. B. World Health Organ. 58, 585–591.
Organization, W.H., 2009. Clinical features of severe cases of pandemic influenza Pandemic (H1N1) 2009 briefing note 13. Clinical Features of Severe Cases of Pandemic Influenza, Geneva, p. 16.
Palese, P., 2004. Influenza: old and new threats. Nat. Med. 10, S82–S87.
Park, J.W., Jo, W.H., 2009. Infiltration of water molecules into the oseltamivir-binding site of H274Y neuraminidase mutant causes resistance to oseltamivir. J. Chem. Inf. Model. 49, 2735–2741.
Pinto, L.H., Lamb, R.A., 2006. The M2 proton channels of influenza A and B viruses. J. Biol. Chem. 281, 8997–9000.
Pizzorno, A., Bouhy, X., Abed, Y., Boivin, G., 2011. Generation and characterization of recombinant pandemic influenza A (H1N1) viruses resistant to neuraminidase inhibitors. J. Infect. Dis. 203, 25–31.
Rungrotmongkol, T., Udommaneethanakit, T., Malaisree, M., Nunthaboot, N., Intharathep, P., Sompornpisut, P., Hannongbua, S., 2009. How does each substituent functional group of oseltamivir lose its activity against virulent H5N1 influenza mutants? Biophys. Chem. 145, 29–36.
Russell, R.J., Haire, L.F., Stevens, D.J., Collins, P.J., Lin, Y.P., Blackburn, G.M., Hay, A.J., Gamblin, S.J., Skehel, J.J., 2006. The structure of H5N1 avian influenza neuraminidase suggests new opportunities for drug design. Nature 443, 45–49.

Ryckaert, J.P., Ciccotti, G., Berendsen, H.J.C., 1977. Numerical integration of the cartesian equations of motion of a system with constraints: molecular dynamics of n-alkanes. J. Comput. Phys. 23, 327–341.
Stephenson, I., Nicholson, K.G., 1999. Chemotherapeutic control of influenza. J. Antimicrob. Chemother. 44, 6–10.
Takeda, M., Leser, G.P., Russell, C.J., Lamb, R.A., 2003. Influenza virus hemagglutinin concentrates in lipid raft microdomains for efficient viral fusion. Proc. Natl. Acad. Sci. U.S.A. 100, 14610–14617.
Tong, S., Li, Y., Rivailler, P., Conrardy, C., Castillo, D.A.A., Chen, L.-M., Recuenco, S., Ellison, J.A., Davis, C.T., York, I.A., 2012. A distinct lineage of influenza A virus from bats. Proc. Natl. Acad. Sci. U.S.A. 109, 4269–4274.
Udommaneethanakit, T., Rungrotmongkol, T., Bren, U., Frecer, V., Stanislav, M., 2009. Dynamic Behavior of Avian Influenza A Virus Neuraminidase Subtype H5N1 in Complex with Oseltamivir, Zanamivir, Peramivir, and Their Phosphonate Analogues. J. Chem. Inf. Model. 49, 2323–2332.
Vavricka, C.J., Li, Q., Wu, Y., Qi, J., Wang, M., Liu, Y., Gao, F., Liu, J., Feng, E., He, J., 2011. Structural and functional analysis of laninamivir and its octanoate prodrug reveals group specific mechanisms for influenza NA inhibition. PLoS Pathog. 7, e1002249.
Von Itzstein, M., 2007. The war against influenza: discovery and development of sialidase inhibitors. Nat. Rev. Drug Discovery 6, 967–974.
Wang, N.X., Zheng, J.J., 2009. Computational studies of H5N1 influenza virus resistance to oseltamivir. Protein Sci. 18, 707–715.
Wang, J.M., Wolf, R.M., Caldwell, J.W., Kollman, P.A., Case, D.A., 2004. Development and testing of a general amber force field. J. Comput. Chem. 25, 1157–1174.
Wang, J.M., Hou, T.J., Xu, X.J., 2006. Recent advances in free energy calculations with a combination of molecular mechanics and continuum models. Curr. Comput. Aided Drug Des. 2, 287–306.
Webster, R.G., Govorkova, E.A., 2006. H5N1 influenza—continuing evolution and spread. N. Engl. J. Med. 355, 2174–2177.
Weiser, J., Shenkin, P.S., Still, W.C., 1999. Approximate atomic surfaces from linear combinations of pairwise overlaps (LCPO). J. Comput. Chem. 20, 217–230.
Woods, C.J., Malaisree, M., Pattarapongdilok, N., Sompornpisut, P., Hannongbua, S., Mulholland, A.J., 2012. Long time scale gpu dynamics reveal the mechanism of drug resistance of the dual mutant I223R/H275Y neuraminidase from H1N1-2009 influenza virus. Biochemistry 51, 4364–4375.
Xu, L., Sun, H., Li, Y., Wang, J., Hou, T., 2013. Assessing the performance of MM/PBSA and MM/GBSA methods. 3. The impact of force fields and ligand charge models. J. Phys. Chem. B 117, 8408–8421.
Xue, W.W., Pan, D.B., Yang, Y., Liu, H.X., Yao, X.J., 2012. Molecular modeling study on the resistance mechanism of HCV NS3/4A serine protease mutants R155K, A156V and D168A to TMC435. Antiviral Res. 93, 126–137.
Yang, Y., Qin, J., Liu, H.X., Yao, X.J., 2011. Molecular dynamics simulation, free energy calcuiation and structure-based 3D-QSAR studies of B-RAF kinase inhibitors. J. Chem. Inf. Model. 51, 680–692.
Yen, H.L., Webster, R.G., 2009. Pandemic influenza as a current threat. Springer, Berlin Heidelberg.
Zhang, J., Hou, T., Wang, W., Liu, J.S., 2010. Detecting and understanding combinatorial mutation patterns responsible for HIV drug resistance. Proc. Natl. Acad. Sci. U.S.A. 107, 1321–1326.